[Revision 2]

Structural changes in shocked tektite and their implications to impact-induced glass formation

Toshimori Sekine[1,2*], Tsubasa Tobase[1], Youjun Zhang[3], Ginga Kitahara[4], Akira Yoshiasa[4], Tomoko Sato[5], Takamichi Kobayashi[6], and Akihisa Mori[7]

[1]*Center for High Pressure Science and Technology Advanced Research, Shanghai 201203, China*

[2]*Graduate School of Engineering, Osaka University, Suita 565-0871, Japan*

[3]*Institute of Atomic and Molecular Physics, Sichuan University, Chengdu 610065, China*

[4]*Graduate School of Science and Technology, Kumamoto University, Kumamoto 860-8555, Japan*

[5]*Deapartment of Earth and Planetary Systems Science, Hiroshima University, Higashi-Hiroshima 739-8526, Japan*

[6]*National Institute for Materials Science, Tsukuba 305-0044*, Japan

[7]*Department of Mechanical Engineering, Sojo University, Kumamoto 860-0082, Japan*

[*]Corresponding author; toshimori.sekine@hpstar.ac.cn

Center for High Pressure Science & Technology Advanced Research (HPSTAR)

1690 Cailun Rd, Pudong, Shanghai 201203, China

ABSTRACT

Heavy meteorite impacts on the Earth surface produce melt and vapor which are quenched rapidly and scattered over wide areas as natural glasses with various shapes and characteristic chemistry, that are known as tektites and impact glasses. Their detailed formation conditions have long been debated in many studies using mineralogical and geochemical data and numerical simulations of impact melt formations. These impact processes are also related to the formation and evolution of planets. To unravel the formation conditions of impact-induced glasses, we performed shock recovery experiments on a tektite. Recovered samples were characterized by X-ray diffraction, Raman spectroscopy, and X-ray absorption fine structure spectroscopy on Ti K-edge. Results indicate that the densification by shock compression is subjected to post-shock annealing that alters the density and silicate-framework structures, but that the local structures around octahedrally coordinated Ti ions remain in the quenched glass. The relationship between the average Ti-O distance and Ti K pre-edge centroid energy is found to distinguish the valance state of Ti ions between Ti^{4+} and Ti^{3+} in the glass. This relationship is useful in understanding the formation conditions of impact derived natural glasses. The presence of Ti^{3+} in tektites constrains the formation conditions at extreme high temperatures or reduced environments. However, impact glasses collected near the impact sites do not display such conditions, but rather relatively mild and oxidizing formation conditions. These different formation conditions are consistent with the previous numerical results on the crater size dependence. (240 words)

46 Keywords: Tektite, shock-recovered tektite, impact conditions, Ti K edge XAFS, local
47 structure of Ti.

INTRODUCTION

Tektites are natural silica-rich glasses found in the strewn fields of impact craters (e.g. Melosh, 2020), whereas impact glasses are found near relatively small craters as the quenched products of impact-induced melts (e.g. Koeberl, 1986). Tektites are relatively in a narrow range of chemical compositions as a whole (Koeberl, 1986). These natural glasses observed on the Earth surface (e.g. Glass, 2016; Wright et al., 1984) and in planetary materials (e.g. Lunning et al., 2016) are all quenched products of melts that were formed at high temperatures. Proposed formation mechanisms include impact generated ejection and cratering of surface rocks and soils, cooling of silicate melt magma, rapid condensation of silicate vapor, cold compressions of silicate crystals, lightning strikes, faulting friction, burning, and heavy irradiation of high energy particles (McCloy, 2019).

The chemistry and structures of these quenched glasses have been studied by various methods and results have shown linkages to the conditions at the time of their formation. However, the mechanism and conditions of tektite formation are still a matter of open inquiry. Unraveling structural changes in glass and melt resulting from the application of dynamic shock pressure requires the knowledge of geochemistry, materials science, and condensed matter physics. The issues involved are very complex because the formation conditions are influenced by a variety of factors including but not limited to morphology, chemical structures, and cooling rate.

The cooling path from a fully equilibrated melt is not instantaneous, and there is no single fictive temperature. Rather a distribution of fictive temperatures has been proposed. Cooling rates range from 10^7 °C/min in submarine basaltic magmas (Potuzak

et al., 2008), to 10^{4}-10^{2} °C/min in tektites (Weeks et al., 1984; Wilding et al., 1996a), and to as slow as 10^{-2}-10^{-4} °C/min in magmatic obsidian flows (Wilding et al., 1996b). In addition, there are two temperature scales: glass temperature (inherently thermodynamic property) and fictive temperature (inherently kinetic property, defined as the temperature at which the glass-forming system has a structural relaxation time equal to an external observation time scale, typically taken as 30–40 s for oxide glasses). Fictive pressure has also been known to relax the densification of silicate glasses in complex ways. Sonnevill et al. (2012) measured the density changes of fused silica glass (FSG) using *in-situ* Raman and Brillouin scattering spectroscopies, and found that permanent densification starts around 9 GPa and ends around 22 GPa.

There are several reports of shock-recovered FSG as illustrated in Fig. S1 (Arndt et al., 1971; Gibbons and Ahrens, 1971; Sugiura et al., 1997; Okuno et al., 1999), as well as the diamond anvil study (Corret et al., 2017). The results on shock recovered samples of 1.2 wt% TiO_2-bearing FSG (Arndt, 1983), and natural glasses (Gibbons and Ahrens 1971; Shimada et al., 2004) show similar changes. Static compression result on FSG at 14 GPa and room temperature (Cornet et al., 2017) is close to the shock results and show that densities above 14 GPa increase linearly and then the increasing rate is saturated around 25 GPa (Polian and Grimsditch, 1990). The shock-recovered samples, however, showed lower densities than the static ones and the peak densities for the shock recovered glasses occur at pressures below ~ 25 GPa (Fig. S1). These reports suggest that relaxation processes in the shock densification of silicate glass may be time-dependent and may not be simple.

While most of the existing literature on tektite is focused on the mineralogy and geochemistry, the formation conditions are not experimentally asserted yet except for a few studies. Macris et al. (2018) performed simulation experiments on mixtures of powdered natural tektite plus quartz grains heated to 1800–2400 ^{o}C for 1–120 s and obtained insights into the thermal history of impact ejecta based on the diffusion between lechatelierite and host glass in tektites in seconds after impact. A maximum temperature of 2360 ^{o}C yields an effective diffusive time scale of ~5 s, a cooling time scale of ~90 s, and a cooling rate at the glass transition temperature of ~5 ^{o}C/s. The results are consistent with the previous estimates for tektites (Weeks et al., 1984; Wilding et al., 1996). Natural intensive impacts, however, are expected to generate much higher temperatures (2800 K to 5700 K) according to the experimental measurements on soda lime glass at pressures of 60 GPa to 110 GPa (Kobayashi et al., 1998).

Previous studies have investigated characteristic glass structures by various methods such as X-ray diffraction (XRD), Raman, X-ray absorption fine structure (XAFS) (e.g. Masleraro and Zanotto, 2018), Infrared spectroscopy (IR) (Morlok et al., 2016), neutron diffraction (Yarker et al., 1986), Mössbauer spectroscopy (Cottrell et al., 2009), nuclear magnetic resonance (NMR) (Ackerson et al., 2020), cathode luminescence (CL) (Gucsik et al., 2004), electron spin resonance (ESR), electron paramagnetic resonance (EPR) (Lombert et al., 2011), atomic force microscopy (Golubev et al., 2018), etc. In particular, Raman spectra measurements on silicate glasses have been used widely to provide information on the local structures of short range and intermediate range around Si atoms (Hemley et al., 1986; McMillan et al.,

1994). The band located around 450 cm^{-1}, called the main band (MB), corresponds to the symmetrical Si–O–Si stretching mode and can be related to the Si–O–Si inter-tetrahedral angle distribution. The defect lines D1 at 490 cm^{-1} and D2 at 606 cm^{-1} are attributed to four- and three-membered SiO_4 ring vibrations, respectively. The vibration bands at 400 to 600 cm^{-1} in and between the tetrahedra are associated with cation motions. Vibration at 800 cm^{-1} involves symmetric motions of adjacent Si atoms with respect to the bridging oxygen. Frequency decreases with the Si-O-Si angle, but the vibration at 900 to 1200 cm^{-1} prevails. The motion of oxygen atoms dominates the spectra and the frequencies increase with the degree of polymerization (Faulques et al., 2001). However, there is no experimental data available to deduce the linkage to the formation conditions using samples obtained at the known experimental conditions.

Regarding specific elements in silicate glasses, XAFS spectroscopy has been used widely to determine their local structures. Ti K-edge X-ray absorption near edge structure (XANES) spectra of titanium oxide crystals contain characteristic patterns depending upon the distortion and coordination number (CN) around Ti ions and valence states of Ti ions, and provide the local structural information around the Ti ions (Waychunas 1987; Farges et al., 1996). In crystals XRD techniques give the detailed structures, but XAFS methods have been used to determine the average local structures around Ti ions in glasses (e.g. Mastelao and Zanotto, 2018). The previous reports indicate a broadband correlation between the pre-edge energy position and relative intensity can be used to estimate the CN of Ti^{4+} in glasses. However, the position shifts, and the relative intensity becomes weak in samples with CN=6, depending on the glass chemistry. Therefore, the relationship between the position and intensity of the Ti K

pre-edge is inherently imperfect because it has been known to be affected significantly by the glass constituents such as Al_2O_3, K_2O, and FeO (Romano et al., (2000) and possible presence of Ti^{3+} in glasses under reduced conditions.

Recent studies on mineral samples produced under reductive conditions indicate the presence of Ti^{3+} coexisting with Fe^{2+} (Sutton et a., 2017). Morinaga et al. (1994) reported that the Ti^{3+} content in silicate glasses depends upon the basicity calculated by the chemical composition in terms of Coulomb force between the cation and oxygen ions based upon the absorption spectra at the peak wavelength of the $^2T_2$-^2E transition of Ti^{3+}. Therefore attention is focused on the presence of Ti^{3+} in glasses, especially natural silicate glasses that experienced various formation conditions. Ti^{3+} content has been known to increase at high temperatures, reduced conditions, and low total Ti concentrations. The ^{57}Fe Mössbauer measurements indicated no evidence for ferric iron in tektites (Rossano et al., 1999), suggesting reduced conditions at their formation.. Farges et al. (1997) showed that tetrahedral Ti^{4+} XANES spectra have a very intense pre-edge peak and that the peak for octahedral Ti^{4+} has much lower intensity and higher centroid energy. Ti^{3+} is expected to be predominantly in octahedral coordination (e.g. Dowty and Clark, 1973; Lombard et al., 2011) and its pre-edge peak will therefore also be of low intensity and at lower centroid energy than that for the octahedral Ti^{4+} (Hwang et al., 2016). The three end members of tetrahedral Ti^{4+}, octahedral Ti^{4+}, and octahedral Ti^{3+} lie at distinct positions on the plot between pre-edge centroid energy and Ti-O distance, because Ti-O distance differs between Ti^{4+} and Ti^{3+}. In the glasses and melts, Ti also forms mostly square pyramids with oxygen atoms (i.e., 5-coordinated Ti) (Farges, 1999). However, the medium range environment around Ti in these glasses is

complex, so contributions to the EXAFS spectra can arise from multiple-scattering from the oxygen environment around Ti.

According to numerical simulations (Melosh, 1989 and 2011) on impact melt formation processes, high velocity impacts over 15 km/s are required to form a significant amount. In such intensive impacts, impact-generated vapor plumes will interact with atmosphere. Considering that tektites were scattered over wide areas covering 300-1000 km from the craters, Melosh (1989) proposed atmospheric blowout mechanism that accelerates and delivers plume materials at a threshold energy of 6.3 x 10^{17} J, which corresponds to large impact craters with diameters over 10 km. But there is no experimental simulation on tektite, and experimental data are needed to understand detailed structural changes of tektites and their formation conditions under hypervelocity impact conditions.

The goal of the present study is to investigate the effects of high-pressure shock-compression on a silicate glass through shock recovery experiments and structural characterizations. Characterizations were carried out with XRD, Raman, and XAFS methods. Results are compared with the earlier data on tektites and impact glasses (Wang et al., 2011 and 2013) to understand their formation conditions.

EXPERIMENTAL METHODS

Natural tektite, originated from Asia, was used as the target sample for the present shock recovery experiments. It had a spheroidal ball shape (~3 cm long axis and ~2 cm max diameter) with roughly wavy surface and was sliced along the long axis into pieces. The pieces (~1 mm thick) were then cut into disks with 12 mm diameter to fit the sample space in a recovery capsule as illustrated in Fig. 1. Sample specimens were

polished on both sides and a few small bubbles were observed on the polished surfaces. The specimen density is 2.20 ± 0.05 g/cm^3, being slightly less than those of the known tektites (Chapman et al., 1964). Part of the sample was crushed and pasted in an agate mortar for 1 hour. The powders (< ~50 μm grain size), pressed into the sample space by a piston at 0.3 GPa, were also used as the starting material and the density estimated by the volume and mass is 1.90 ± 0.10 g/cm^3. Sample was set within a stainless steel (SUS304) container (24 mm diameter x 30 mm length) and backed up by a SUS 304 screw. The sample was located 3 mm deep from the impact surface of the container, as illustrated in Fig. 1.

Chemical composition of the starting tektite (TK0 in Table 1) was determined by an electron microprobe analyzer, JOEL EPMA JXA-8200, and compared with other selected natural glasses having similar compositions (Table 1). The composition and Raman data (shown later) on our tektite are similar to those similar to those of australianite tektite, respectively. The Raman was close to that of FSG, too.

A propellant gun at National Institute for Materials Science, Japan (Sekine, 1997) was used to accelerate a 29-mm diameter disk flyer consisting of either 3-mm thick aluminum alloy (Al 6061), 2-mm thick SUS 304, or 2-mm thick tungsten (W) to a required impact velocity. Impact velocity was measured with magnet flyer method. Figure 2 is a summary of pressure (P)-particle velocity (Up) relations of flyer, container, and the sample for the impact velocities of 0.899 km/s, 0.981 km/s, 1.386 km/s, and 1.400 km/s. Pressure is calculated by the impedance math method using measured impact velocity and the known Hugoniot data for Al6061, SUS304, and W (Marsh, 1980). The shock velocity (U_S in km/s) and particle velocity (U_P in km/s) relationships

were; $U_S = 5.35 + 1.34U_P$ for Al6061 (2.703 g/cm^3), $U_S = 4.58 + 1.49U_P$ for SUS304 (7.89 g/cm^3), and $U_S = 4.04 + 1.23U_P$ for W (19.2 g/cm^3). We assumed that the tektite Hugoniot can be represented by that of fused silica glass (FSG), given by $U_S = 5.05 + 0.001U_P$ for $Up < 27$ GPa and $U_S = 0.95 + 1.66U_P$ for $Up > 27$ GPa. Pressure and density are calculated by the Rankine-Hugoniot equations (Table 2) using $P = \rho_0 U_S U_P$ and $\rho = \rho_0 Us/(Us-Up)$, where P, ρ, and ρ_0 are pressure, density, and zero-pressure density, respectively. Figure 2b illustrates the pressure history profiles, calculated by Autodyne code (2D v12.1), at the central, middle section of the sample. The history profiles show a stepwise increase to reach the peak pressures at ~ 1.4-1.5 μs after 3-4 times reflections within sample and subsequently drop. For powdered samples, we assumed the peak pressure reached the equilibrium pressure with the container. The post-shock temperatures were calculated by Gibbons and Ahrens (1971) method, as listed in Table 2. These pressure and temperature will have large variations in powders (Bland et al., 2014) and we pay attention to explain the results for the recovered samples.

The recovered containers were cut open using a lathe to collect the samples. We removed particles of Al6061, SUS304, and W as completely as possible. Recovered samples were investigated using XRD, Raman spectroscopy, and XAFS techniques. XRD powder patterns were scanned in a range of 10 to 90 degree in 2 theta at 2 degrees per second with Cu Kα radiation at 40 kV and 40 mA. Raman data calibrated by Si (520 cm^{-1}) were measured using a Renishaw inVia Raman microscope equipped with a probe beam (~1 μm diameter) of 532 nm and 9 mW without any damage under an optical microscope. XAFS measurements were collected from an area (~1 mm x ~1 mm) of powders on plastic tape and performed at beamline BL-9C with Si (111) double-crystal

monochromator of the Photon Factory, KEK, Japan. Spectra were recorded in the transmission mode at room temperature in an energy rage between 4564.4 eV and 5355.0 eV. The detailed measurement method was same as described by Wang et al. (2011). XAFS spectra were analyzed by XAFS 93 and MBF 93 programs (Yoshiasa et al., 1999). The radial structural function was obtained by the Fourier transform over the k range of 3.0 $Å^{-1} < k < 12.0$ $Å^{-1}$ or 2.5 $Å^{-1} < k < 11.0$ $Å^{-1}$, but the results did not show significant variations in the results. In the quantitative analysis for samples (TK0 - TK4, TKP1, and TKP2), we performed a Fourier filtering technique and a non-linear least squares structure parameter fitting method with an analytical EXAFS formula (Maeda, 1987). In order to obtain information around the structure parameters, we conducted parameter fitting with analytical EXAFS formulae. For reference, we performed same measurements on TiO, TiO_2, and Ti_2O_3 as well.

EXPERIMENTAL RESULTS

All the experimental conditions are summarized in Table 2. Four bulk samples (TK1 to TK4) and 2 powdered samples (TKP1 and TKP2) were studied at pressures from 10 GPa to 35 GPa. Powdered samples are generally heated more than the bulk at a shock pressure, and the two were added to check the temperature effects (Bland et al., 2014).

XRD patterns

Figure 3 shows XRD patterns over the range of 2θ of 15 to 35 degrees that have a broad peak in each sample profile. The starting sample is a glass with a broad band centered around 22 degrees. The recovered samples also remained completely glasses. The broad peaks shift slightly to high angles with increasing pressure to 10 GPa (TK1)

and 17 GPa (TK2), but moves back nearly to that of the initial sample (TK0) at 35 GPa (TK4). The powdered initial samples (TKP1 and TKP2) show nearly identical shift to those of TK2 and TK3. The XRD results are consistent with the previous results (Shimoda et al., 2001) that shocked FSG and obsidian glass remain glasses after the shocks similar to the present study. Recent *in-situ* XRD results on shock-compressed fused silica also indicated that the fused silica below 34 GPa does not show any sharp peaks (Tracy et al., 2018). A strong and sharp peak was observed around 41 degrees is attributed to contamination of W particles in TK4 only (not shown). The broad peak in TK4 appears to sharpen relatively and this sample was checked using a scanning electron microscopy coupled with element analysis system. The results (Fig. S3) show no oxide crystal except for alumina fine grains used in polishing, but Fe-Cr-Ni-Mn alloy grains in glass were detected additionally as relicts of sample container.

RAMAN spectroscopy

Figure 4 shows Raman spectra. The starting tektite displays peaks of MB, D1, D2, ~790 cm^{-1}, ~900 cm^{-1}, and ~1010 cm^{-1}, which are very similar to those for Australite (Faulgues et al., 2001). The D2 band around 580 cm^{-1} becomes clear in TK2 and as a whole all the peaks shift slightly to a high wave number. The spectra from samples TK3 and TK4 show strong D1 bands. For the powdered samples (TKP1 and TKP2), the peak around 1100 cm^{-1} becomes sharp and strong and the D2 band is enlarged remarkably in TKP1. Except for the strong 1100 cm^{-1} peaks, TKP2 is similar to TK4. These results correspond to the global structural changes in silicate networks. The D1 bands of TK3, TK4, and TKP2 at high pressures are clear relative to those of the others.

XAFS measurements

Figure 5 compares the measured Ti K-edge XAFS patterns of shocked samples calibrated by Ti foil pre-edge energy (4964.9 eV). Included are reference compounds of rutile (TiO_2-r), anatase (TiO_2-a), NaCl-type TiO, and corundum-type Ti_2O_3. The starting tektite consists of typical tetrahedral Ti^{4+} ions (Table 3) as characterized by the pre-edge features (Ackerson et al., 2020). All the patterns in Fig. 5, except for TK3 and TK4, are similar to that of the starting sample, and the pre-edge intensities for TK3 and TK4 are reduced greatly (Fig. 5b) after the normalization by the peak height at 5 keV. TKP1 is similar to TK2 in the pre-edge intensity, and TKP2 is rather similar to TK0 and TK1 (Fig. 5b). The pattern for TK4 is completely different from the others and very similar to that of anatase. TK3 is intermediate between TK4 and the others (Fig. 5b).

Calculated Ti-O distances are listed in Table 3 together with the pre-edge peak position and relative intensity. The EXAFS is illustrated in Fig. S2. For the powdered samples (TKP1 and TKP2), the changes observed by Raman spectra are not clearly seen in the Ti local structure of the tektite samples. The structural changes in silicate networks by the Raman measurements differ from those seen in the Ti K-edge XAFS. TiO and Ti_2O_3 have very weak pre-edge peaks with lower energy positions than TiO_2.

DISCUSSION

We have performed shock-recovery experiments on a typical tektite and the recovered samples were investigated by XRD, Raman spectroscopy, and Ti K-edge XAFS methods. Our focus was on structural changes in a silicate glass by shock compression to constrain the formation conditions of various natural glasses formed by impacts such as tektites and impact glasses.

Changes in silicate glass by impacts

The calculated peak density based on the FSG Hugoniot indicates a monotonic increase in density with increasing peak pressure (Table 2), but the previous reports confirmed the presence of a maximum density around 25 GPa (Fig. S1) for various silica-rich glasses (Gibbons and Ahrens, 1971, Shimada et al., 2004, Manghnani et al., 2011). These studies were based on refractive index measurements, XRD, and Raman spectroscopy methods, and the presence of the density peaks was attributed to the annealing during the adiabatic release process. When shock pressures are above 20 GPa, the post-shock temperatures are known to be high enough to anneal the densification (Gibbons and Ahrens, 1971). However, considering that the density change subjected to the annealing effects is associated mainly with the SiO_4 tetrahedron linkage, it will be difficult to understand the structural changes in the post shock silicate glass based solely on the results with XRD and Raman methods. Therefore, further direct, local structural information of silicate glass is required to understand unambiguously the residual effects in the post shock silicate glass, when one evaluates the formation and quenching processes of natural glasses subjected to the residual effects.

The starting tektite displays a Raman pattern similar to those of FSG, australianite, indochinite, and obsidian (Faulgue et al., 2001). Raman data on the shock-recovered tektite reported in the present study are first of its kind, and there are seen significant changes in the peak intensity variation both at peak shock pressures and between bulk and powder samples. The most remarkable changes are seen in the powder samples at pressure ranges similar to those for the bulk. Faulgue et al. (2001) characterized natural glasses including tektites and impact glasses by Raman and IR spectroscopies. When one compares Raman data between our powdered samples and natural tektites, the

recovered powders are similar to two tektites of moldavite (Bohemia) and Cau-Ca valley (Columbia) with sharp peaks around 450 cm^{-1} and 1075 cm^{-1} (Faulgues et al., 2001). These peaks are related to the Si–O–Si inter tetrahedral angle, and the frequency at 1000-1100 cm^{-1} was observed to be the largest in TKP1 that was quenched at a relatively low pressure and a high temperature. The broad band at 1000 cm^{-1} to 1600 cm^{-1} is related to the substitutions of silicon by metals (e.g. Al). A comparison of Raman spectra between the bulk and the powder samples at similar shock pressures suggests that temperature effect is more important than pressure in affecting the tektite glass structure. It is noteworthy that powdered samples display characteristic Raman peaks affected by the high residual temperature due to the initial porosity and that they differ from those of the starting and recovered bulk samples. This suggests that some natural tektites were quenched rapidly from higher residual temperatures than those in the present experiments.

The variation in the D1 (~490 cm^{-1}) and D2 (~600 cm^{-1}) bands for TKP1 differs from the others, and is related to the four- and three-membered SiO_4 ring vibrations, respectively. XRD and Raman data by themselves are insufficient to determine silicate glass structures unambiguously because there are different structural features among natural glasses (Faulgues et al., 2001) that are subjected to annealing in the glass formation process.

Local structural changes around Titanium in glass

Ti in silicate glasses is present as various species. Ti-bearing silicate glasses obtained at high pressures showed a density increase with increasing pressure (Arndt, 1983), but Paris et al. (1994) demonstrated no change in the Ti K pre-edge feature.

Although Ti K-edge has been used to determine the CN from the pre-edge position and intensity, it is not clear whether Ti K pre-edge feature is enough to distinguish species or not. It has been known that Ti can be present as Ti^{3+} as well as Ti^{4+} depending upon the formation condition and chemical composition. The pre-edge features for TiO and Ti_2O_3 are very weak as well as that of TiO_2 (Fig. 5), although all of them are coordinated with six oxygen atoms. Therefore it is difficult to distinguish between Ti^{4+} and Ti^{3+} from a comparison of the pre-edge features if they coexist in natural glasses. When we take an average distance of Ti-O in silicate glass, the ionic radii of Ti with CN=6 are 0.605 Å, 0.670 Å, and 0.86 Å for Ti^{4+}, Ti^{3+}, and Ti^{2+} (Shannon, 1976), respectively. The previous Ti K edge XANES and EXAFS studies on some typical Ti-bearing crystals (Berry et al., 2007; Ackerson et al., 2020) reported the relationship between the coordination of Ti^{4+} and the average Ti-O distance. They summarized that the Ti^{4+}-O distances for CN=6 and CN=4 are 1.96-2.085 Å and 1.804-1.835 Å, respectively. From XANES analysis, we determined the average Ti-O distances in shock-recovered silicate glasses (Table 3) and plotted them in Fig. 6 in comparison with those of some natural glasses (7 tektites, 2 impact glasses, and 2 volcanic glasses) reported previously (Wang et al., 2011 and 2013) as listed in Table S1. It may be seen in Fig. 6 that the present starting tektite (Tk0) and tektite samples from Wang et al. (2011 and 2013) are located in a range of Ti-O distance of 1.81-2.00 Å at a constant energy position near 4968 eV. When one compares the data between the present recovered samples (Table 2) and natural glasses (Table S1), two different trends are seen in Fig. 6. (i) A trend of having Ti^{4+} to TiO_2 for the results on the present shock-recovered tektite samples as well as the volcanic glasses and impact glasses

(Wang et al., 2013). (ii) Another trend of having Ti^{3+} to Ti_2O_3 for natural tektites. The trend (i) can be explained simply by coordination increase of Ti^{4+}. The latter trend (ii) cannot be explained by only Ti^{4+} and is indistinguishable in the plot of energy-intensity for Ti K pre-edge peaks (Ackerson et al., 2020). The present maximum experimental pressure was 35 GPa and achieved by the multiple shock reflection. Thus the temperature was not high enough to reduce Ti^{4+} into Ti^{3+}. But a small amount of Ti^{3+} may be present.

Measured shock temperatures on soda lime glass, which is comparable to a similar silicate glass, indicated ~3000 K at 60 GPa and 5700 K at 110 GPa by a single shock wave (Kobayashi et al., 1998). Shock compressions without reflection may approximate natural impact conditions and the temperature will reach over 3000 K. Although the previous reports (Wang et a., 2011 and 2013) assumed all Ti^{4+} and explained by CN changes of Ti^{4+} only, the present plot (Fig. 6) displays distinct trends for Ti^{4+} and Ti^{3+}. The recovered samples are located in trend (i) and indicate that the coordination of Ti atoms increases at high shock pressures. The two volcanic glasses (v1 and v2 in Fig. 6) display the 5-fold Ti^{4+} and one of impact glass (m2 in Fig. 6) show a deviation from the trend (i), but the reason is not clear either structural changes in Ti^{4+} or partial reduction to Ti^{3+}. Simon et al. (2007) reported that Ti^{3+} has a large distribution coefficient between solid and liquid and can be concentrated into liquid during crystallization. Ti^{3+} may prefer to be in the quenched glass over the crystal state.

Formation at extreme conditions

Moldavite is a tektite characterized by negligible water content and few vesicles and has been considered as originated at the time of the formation of Ries crater.

According to Engelhardt et al. (1987), the only lithology from which moldavites could have been formed is Middle Miocene sands, which formed a thin veneer in the Ries area at the time of the impact. Enrichments and depletions of individual elements in moldavites cannot be explained by fractional vaporization (Žák et al., 2016). This was confirmed also by melting and evaporating experiments with sand samples (Konta and Mráz, 1975). Moreover, the negligible water content in moldavites and the scarcity of vesicles excludes the formation of moldavite melt by simple fusion of sands. In the expanding and ascending vapor liquid droplets are condensed in the quenching process. The color of moldavites is characterized by the composition and poverty in leachatelierite and bubbles (Bouška and Ulrych, 1984); brown ones are rich in Al_2O_3 and total Fe, with low $Fe^{2+}/\Sigma Fe$, and poor in SiO_2, and green ones are rich in SiO_2 and poor in Al_2O_3 and total Fe with high $Fe^{2+}/\Sigma Fe$. This may suggest the brown moldavites were formed at relatively oxidizing conditions than the green moldavites. Oxygen fugacities (fo_2) were measured for indochinites between 650 °C and 850 °C by Walter and Doan (1969) and a bediasite between 481 °C and 990 °C by Brett and Sato (1984). Application of an equation on Fe^{3+}/Fe^{2+} ratios in natural silicate liquids depending on oxygen fugacity, temperature, and chemical composition (Sack et al., 1980) results in $fo_2 = 10^{-15.9}$ atm at 800 °C and $10^{-0.51}$ atm at 3000 °C, respectively, for moldavites with $Fe^{3+}/Fe^{2} = 0.10$ (i.e. $Fe^{2+}/\Sigma Fe = 0.91$). These estimations may suggest that they were formed and quenched at very reduced and high temperature states. Cathodoluminescence (CL) of moldavites (Fritzke et al., 2017) distinguished between different shapes of green CL spectra in the matrix of the tektite glasses and blue color for lechatelierite inclusions (a pure silica-glass phase). The visible green CL emission is

caused by defects related to strong local disorder as well as Al-O^--Al defects. The blue CL emission is activated by different types of lattice defects such as nonbridging oxygen-hole centers, self-trapped excitons, and oxygen deficiency centers. These defects can enhance to produce reduction in Ti at high temperatures and reduced conditions.

Redox in silicate melts

The redox states of iron and titanium have been investigated in silicate melts using Mössbauer and optical absorption methods by Nolet (1980) and Schreiber et al. (1982). The silicate compositions were basaltic, relatively SiO_2-poor, but the coexisting pairs of Fe^{2+} and Ti^{3+} in the melts or Fe metal and Ti^{4+} were recognized experimentally and theoretically. The coupling pairs were explained by the crystal-field absorption and the charge transfer transition. They concluded that Fe^{2+} and Ti^{3+} do not coexist under reduced conditions where metallic iron is stable in the silicate melts and that Ti^{3+} ions occupy the octahedral sites. The reaction may be represented by Fe^{2+} (in melt) + 2 Ti^{3+}(in melt) = Fe (solid) + 2 Ti^{4+} (in melt). This means the iron amount should be in excess of that of titanium in melts. The Fe^{2+} and Ti^{3+} may coexist in melts because the oxidation of Ti is considerably sluggish relative to Fe under some circumstances (Simon et al., 2016). The EPR study on Ti^{3+} in silicate glasses (Lombard et al., (2011)) revealed the presence of five-fold Ti^{3+} ions in the trigonal bi-pyramids that is intermediate between the square-based pyramidal and octahedral configurations.

As a network former, ferric iron Fe^{3+} must connect more tightly to other network formers (Si and Al). Ferrous iron Fe^{2+} is surrounded by dominantly non-bridging oxygens, which results in more ionic bonds to its neighbors, on average (Farges et al.,

2004). Ti works as network former with CN=4 and CN=6 (modifier for the excess Ti) if SiO_2 is not enough, and Ti with CN=4 disappears and becomes CN=5 in glasses as modifier. ^{57}Fe Mössbauer spectroscopy of tektites (moldavite and australianite) (Rossano et al., 1999) indicated four- and five-fold ferrous irons without ferric iron. TiO_2 plays complicated roles depending upon the concentration. This differs between crystals and glasses. Faulques et al., (2001) reported a difference in Raman patterns between tektite, impact glasses, and obsidian to suggest higher crystallinity in tektites. Recent nano scale observations, however, reveal heterogeneity in natural impact glasses (Golubev et al., 2018). Therefore we need further study to unravel the two trends as indicated in Fig. 6, but for our purpose to constrain the formation condition we can use the relation between the Ti-O distance and the pre-edge energy position.

Variations in tektite formation conditions

Considering reduction of Ti at high temperatures, the distinct trends of Fig. 6 suggest a significant variation of the formation conditions of tektites, especially for moldavite-green and other tektites. Previously their long average Ti-O distances determined by XAFS measurements were explained by 6-fold coordination of Ti^{4+} (Wang et al., 2011 and 2013), but the present study unravels the presence of Ti^{3+} in such glasses and indicates their reductive formation conditions. The reductive conditions can be relevant to the difference between some tektites and impact glasses. Tektites observed in wide fields are considered to have faster initial ejecta speeds than impact glasses found only near the impact sites. Fast ejecta speeds can help tektite precursors (melt and/or vapor) to bring up to low oxygen atmosphere with intense frictional heating by atmosphere in travel and may produce large amounts of tektites in

large-scale impacts. On the other hand, slow ejecta speeds may produce relatively small amounts of melts and suggests relatively mild impact conditions. According to numerical simulations (Melosh, 2011; Luther et al., 2019), the difference in the formation conditions can be explained in terms of the crater size and the ratio of impactor (projectile) to target (surface rock). Geochemical data of minor elements in tektites supports very low components of projectile because large crater formations involve interactions with significant amounts of deep rocks.

Recent mineralogical studies have indicated the presence of high-pressure minerals in some tektites (e.g. McCloy, 2019), supporting their experience not only at high temperatures but also at high pressures. Most of tektites and impact glasses containing the tetrahedral Ti^{4+} only, however, may suggest their different formation mechanisms from those formed at extreme conditions like green moldavites. They might have been formed from the Earth surface rocks melted by thermal pulses, associated with reactions in air near the Earth surface at the time of entry of hypervelocity projectile, and quenched after the thermal wave receded. The implication remains to be verified by further studies.

IMPLICATIONS

The structural changes in the shock-recovered tektite samples were investigated as a function of pressure through XRD, Raman, and XAFS measurements. In addition to the SiO_4-tetrahedral network structures in the glasses, Ti local structures in the shock-recovered samples were compared with those of the reference crystals of TiO, TiO_2, and Ti_2O_3 and the previous reports on tektites and impact glasses on the plot between Ti K pre-edge peak energy position and average Ti-O distance. Although the

484 experimentally-shocked tektites displayed an increase in coordination number of Ti ions,
485 they did not duplicate the natural tektite features previously reported. Two distinct
486 trends, however, were found in the plot regarding the presence of Ti^{3+} and Ti^{4+} in the
487 natural silicate glasses, suggesting their different formation conditions. We conclude the
488 following implications:

489 1. Densification of tektite by shock compression is subjected to annealing in the
490 release process, as reported by previous studies, but the local structures around
491 Ti can be quenched in recovered samples (Fig. 6). Therefore, the Ti local
492 structures in impact glasses are useful to estimate their formation conditions
493 and impact scales.
494 2. Some tektites like green moldavites may have been subjected to intensive
495 heating by impact, probably more than ~3000 K and condensed from
496 impact-produced plumes. Reduction to Ti^{3+} in melts may remain partially or
497 totally in the quenched glass because the redox reaction in Ti is sluggish
498 relative to that in iron.
499 3. Impact glasses observed near impact sites also may be the quenched melts that
500 are formed by relatively mild impacts without significant reduction, suggesting
501 impact heating probably below ~3000 K.
502 4. It is probable that some tektites and impact glasses with the tetrahedral Ti^{4+}
503 only could be formed by the thermal wave near the Earth surface.

504

505 **Acknowledgments**

506 Shock experiments were carried out at National Institute for Materials Science as

507 collaboration researches. XRD and Raman Measurements were conducted at HPSTAR.
508 EPMA analysis was conducted at Hiroshima University. XAFS measurements were
509 performed at the Photon Factory Project PAC (No. 2019G631). We are thankful to Yuki
510 Horie to read for improving our expressions. This research was in part supported by
511 NSFC (41974099) and JSPS (18H01269). Editors and three reviewers made helpful
512 comments to improve the draft.

513

514

515 **References**

516

517 Ackerson M. R., Cody G. D., and Mysen B. O. (2020) ^{29}Si solid state NMR and Ti
518 *K*-edge XAFS pre-edge spectroscopy reveal complex behavior of Ti in silicate
519 melts. Progress in Earth and Planetary Science, 7, 14.

520 Alexander C.S., Chhabildas, L.C., Reinhart W.D., and Templeton W.D. (2008) Changes
521 to shock response of fused quartz due to glass modification. International Journal of
522 Impact Engineering, 35, 1376-1385.

523 Amano S., Bogdanovski D., Yamane H., Terauchi M., and Dronskowski R. (2016)
524 ε-TiO, a Novel Stable Polymorph of Titanium Monoxide. Angewandte Chemie
525 International Edition, 55, 1652 –1657.

526 Arndt J., Hornemann U., and Müller W.F (1971) Shock-wave densification of silica
527 glass. Physics and Chemistry of Glasses, 12, 1-7.

528 Arndt J. (1983) Densification of glasses of the system TiO_2-SiO_2 by very high static
529 pressures. Physics and Chemistry of Glasses, 24, 104-110.

Berry A.G., Walker A.M., Hermann J., O'Neil H. St.C., and Gale J.D. (2007) Titanium substitution mechanisms in forsterite. Chemical Geology, 242, 176-186.

Bland P.A., Collins G.S., Davison T.M., Abreu N.M., Ciesla F.J., Muxworthy A.R., and Moore J. (2014) Pressure-temperature evolution of primordial solar system solids during impact-induced compaction. Nature Communications, 5, 5451.

Brett R. and Sato M. (1984) Intrinsic oxygen fugacity measurements on seven chondrites, a pallasite, and a tektite and the redox state of meteorite parent bodies. Geochimica et Cosmochimica Acta, 48, 111-120.

Bouška V. and Ulrych J. (1984) Electron microscoprobe anakyses of two-colored moldavites. Journal of Non-Crystalline Solids, 67, 375-381.

Chapman D.R., Larson H.K., and Scheiber L.C. (1964) Population polygons of tektite specific gravity for various localities in Australasia. Geochimica et Cosmochimica Acta, 28, 821- 839.

Cornet A., Martinez V., de Ligny D., Champagnon B., and Christine Martinet (2017) Relaxation processes of densified silica glass. Journal of Chemical Physics, 146, 094504.

Cottrell E., Kelley K.A., Lanzirotti A., and Fischer R.A. (2009) High-precision determination of iron oxidation state in silicate glasses using XANES. Chemical Geology, 268, 167-179

Dowty E. and Clark J.R. (1973) Crystal structural refinement and optical properties of a Ti^{3+} fassaite from the Allemde meteorite. American Mineralogist, 58, 230-242 (and Reply 962-964).

Engelhardt W.V., Luft E., Arndt J., Schock H., and Welskirchner W. (1987) Origin of

553 moldavites. Geochimica et Cosmochimica Acta, 51, 425-443.
554 Farges, F., Brown, Jr. G.E., and Rehr, J.J. (1996) Coordination chemistry of Ti (IV) in
555 silicate glasses and melts: I. XAFS study of titanium coordination in oxide model
556 compounds. Geochimica et Cosmochimica Acta, 60, 3023-3038.
557 Farges F., Brown Jr. G.E., and Rehr J.J. (1997) Ti K-edge XANES studies of Ti
558 coordination and disorder in oxide compounds: Comparison between theory and
559 experiment. Physical Review, B 56, 1809-1819.
560 Farges F. (1999) A Ti K-edge EXAFS study of the medium range environment around
561 Ti in oxide glasses. Journal of Non-Crystalline Solids, 244, 25-33.
562 Farges F., Lefre`re Y., Rossano S., Berthereau A, Calas G, and Brown Jr. G.E. (2004)
563 The effect of redox state on the local structural environment of iron in silicate
564 glasses: a combined XAFS spectroscopy, molecular dynamics, and bond valence
565 study. Journal of Non-Crystalline Solids, 344, 176-188
566 Faulgues E., Fritsch E., and Ostrpumov M. (2001) Spectroscopy of natural silica-rich
567 glasses. Journal of Mineralogical and Petrological Sciences, 96**,** 120-128.
568 Fritzke B., Göteze J., and Lange J.M. (2017) Cathodoluminescence of moldavites.
569 Meteoritics and Planetary Science, 52, 1428-1436.
570 Gibbons R.V. and Ahrens T.J. (1971) Shock metamorphism of silicate glasses. Journal
571 of Geophysical Research, 76, 5489-5498.
572 Glass B. P. (2016) Glass: The geologic connection. International Journal of Applied
573 Glass Science, 7, 435-445
574 Golubev Y.A., Shumilova T.G., Isaenko S.I., Makeev B.A., Utkin A.A., Suvorova E.I.,
575 and Ernstson K, (2018) Nano-heterogeneity of natural impact silica-rich glasses

according to atomic force microscopy and spectroscopy data. Journal of Non-Crystalline Solids, 500, 388-400.

Gucsik A., Koeberl C., Brandstätter F., Libowitzky, and M. Zhanget, (2004) Infrared, Raman, and cathodeluminescence studies of impact glasses. Meteoritics and Planetary Science, 369, 1273-1285.

Hemley R. J., Mao H.K., Bell P.M., and Mysen B.O. (1986) Raman spectroscopy of SiO_2 glass at high pressure. Physical Review Letters, 57, 747-750.

Hwang I., Jiang B., Jin Z., Park C., and Han S. (2016) Anomalous structural disorder and distortion in metal-to-insulator-transition Ti_2O_3. Journal of Applied Physics, 119, 014905.

Kobayashi T., Sekine T., Fat'yanov O.V., Takazawa E., and Zhu Q.Y. (1998) Radiation temperatures of soda-lime glass in its shock-compressed liquid state. Journal of Applied Physics, 83, 1711-1716.

Koeberl C. (1986) Geochemistry of tektites and impact glasses. Annual Review of Earth and Planetary Science, 14, 323-350.

Konta J. and Mráz L. (1975) Volatility of oxides from silicate melt and the origin of moldavites. Mineralogical Magazine, 40, 70-78.

Lombard P., Ollier N., and Boizot B. (2011) EPR study of Ti^{3+} ions formed under beta irradiation in silicate glasses. Journal of Non-Crystalline Solids, 357, 1685-1679.

Lunning N.G., Corrigan C.M., McSween Jr. H.Y., Tenner T.J., Kita N.T., and Bodnar R.J. (2016) CV and CM chondrite impact melts. Geochimica et Cosmochimica Acta, 189, 338-358.

Luther R., Artemieva N., and Wunnemann K. (2019) The effect of atmospheric

599 interaction on impact ejecta dynamics and deposition. Icarus, 333, 71-86.

600 Macris C.A., Asimow P.D., Badro J., Eiler J.M., Zhang Y., and Stolper E.M. (2018)
601 Seconds after impact: Insights into the thermal history of impact ejecta from
602 diffusion between lechatelierite and host glass in tektites and experiments.
603 Geochimica et Cosmochimica Acta, 241, 69-94.

604 Maeda H. (1987) Accurate bond length determination by EXAFS method. Journal of
605 Physical Society Japan, 56, 2777-2787.

606 Manghnani M.H., Husher A., Sekine T., Wu J., Stebbins J.F. and Williams Q. (2011)
607 Raman, Brillouin, and nuclear magnetic resonance spectroscopic studies on
608 shocked borosilicate glass. Journal of Applied Physics, 109, 113509.

609 Marsh S. P. (1980) LASL Hugoniot Data, Univerty of California Press, Berkeley.

610 Masleraro V.R. and Zanotto E.D. (2018) X-ray absorption fine structure (XAFS) studies
611 of oxide glasses-a 45-year overview. Materials, 11, 204.

612 McCloy J. (2019) Frontiers of ntural and un-natural glasses: An interdisciplinary
613 dialogue and review. Journal of Non-Crystalline Solids X, 4, 100035

614 McMillan P.F., Poe B.T., Gillet Ph., and Reynard B. (1994) A study of SiO_2 glass and
615 supercooled liquid to 1950 K via high-temperature Raman spectroscopy.
616 Geochimica et Cosmochimica Acta, 58, 1653-1664.

617 Melosh H.J. (2020) The Australiasian tektite source crater: Found at last? Proceedings
618 of National Academy Sciences of the United States of America, 117, 1252-1253.

619 Melosh H.J. (2011) Planetary Surface processes, Cambridge University Press, New
620 York.

621 Melosh H.J. (1989) Impact cratering a geological process, Oxford University Press,

New York.

Morinaga K., Yoshida H., and Takeba H. (1994) Compositional dependence of absorption spectra of Ti^{3+} in silicate, borate, and phosphate glasses. Journal of American Ceramic Society, 77, 3113-3118.

Morlok A., Stojic A., Weber I., Hiesinger H., Zanetti M., and Helbert J. (2016) Mid-infrared bi-directional reflectance spectroscopy of impact melt glasses and tektites. Icarus, 278, 162-179.

Nolet D.A. (1980) Optical absorption and Mössbauer spectra of Fe, Ti silicate glasses. Journal of Non-Crystalline Solids, 37, 99-110

Okuno M., Reynard B., Shimada Y., Syono Y., and Willaime C. (1999) A Raman spectroscopic study of shock-wave densification of vitreous silica. Physics and Chemistry of Minerals, 26, 304-311.

Paris E., Dingwell D.B., Seifer F.A., Mottana A., and Romano C. (1994) Pressure-induced coordination change of Ti in silicate glass: A XANES study. Physics and Chemistry of Minerals, 21, 510-515.

Polian A. and Grimsditch M. (1990) Room-temperature densification of a-SiO_2 versus pressure. Physical Review, B 41, 6086-6087.

Potuzak M., Nicols A.R.L., Dingwell D.B., and Clauge D.A. (2008) Hyperquenched volcanic glass from Loihi Seamount, Hawaii. Earth and Planetary Science Letters, 270**,** 54-62.

Romano C., Paris E., Poe B.T., Giuli G., Dingwell D.B., and Mottana A. (2000) Effect of aluminum on Ti-coordination in silicate glasses: a XANES study. American Mineralogist, 85, 108-117.

Rossano S., Balan F., Morin G., Bauer J.-P., Calas G., and Brouder C. (1999) ^{57}Fe Mossbauer spectroscopy of tektites. Physics and Chemistry of Minerals, 26, 530-538.

Sack R.O., Carmichael I.S.E., Rivers M., Ghiorso M.S., (1980) Ferric-ferrous equilibria in natural silicate liquids at 1 bar. Contributions to Mineralogy and Petrology, 75, 369-376.

Schreiber H.D., Balazs G.B., Shaffer A.P., and Jameon P.L. (1982) Iron metal production in silicate melts through the direct reduction of Fe(II) by Ti(III), Cr(II), and Eu(I1). Geochimica et Cosmochimica Acta, 46, 1891-1901.

Sekine T. (1997) Shock wave chemical synthesis. European Journal of Solid State Inorganic Chemistry, 34, 823-833.

Shanon R.D. (1976) Revised effective Ionic radii and systematic Studies of Interatomic Distances in halides and chaleogenides. Acta Crystallography, A32, 751-766.

Shimada Y., Okuno M., Syono Y., Kikuchi M., Fukuoka K., Koyano M., and Katayama S. (2004) Structural evolutions of an obsidian and its fused glass by shock-wave compression. Physics and Chemistry of Minerals, 31, 532-542.

Simon S.B., Sutton S.R., and Grossman L. (2007) Valence of titanium and vanadium in pyroxene in refractory inclusion interiors and rims. Geochimica et Cosmochimica Acta, 71, 3098-3118.

Simon S.B., Sutton S.R., and Grossman L. (2016) The valence and coordination of titanium in ordinary and enstatite chondrites. Geochimica et Cosmochimica Acta, 189, 377-390.

Sonnevill C., Mermet A., Chanpagnon B., Mertinet C., Margueritat J., deLigny D.,

668 Deschamps T., and Balima F. (2012) Progressive transformations of silica glass
669 upon densification. Journal of Chemical Physics, 137, 124505.
670 Sugiura H., Ikeda R., Kondo K., and Yamadaya T. (1997) Densified silica glass after
671 shock compression. Journal of Applied Physics, 81, 1651-1655.
672 Sutton S.R., Goodrich C.A., and Wirick S. (2017) Titanium, vanadium and chromium
673 valences in silicates of ungrouped achondrite NWA 7325 and ureilite Y-791538
674 record highly-reduced origins. Geochimica et Cosmochimica Acta, 204, 313-330.
675 Tracy S.J., Turneaure S.J., and Duffy T.S. (2018) In situ x-ray diffraction of shock
676 compressed fused silica. Physical Review Letters, 120, 135702.
677 Walter L.S. and Doan A.S. (1969) Determination of the Po; T equilibrium of
678 indochinite tektites. Meteoritics, 4, 295-296.
679 Wang L., Yoshiasha A., Okuba M., and Takeda T. (2011) Titanium local structure in
680 tektite probed by X-ray absorption fine structure spectroscopy. Journal of
681 Synchrotron Radiation, 18, 885-890.
682 Wang L., Yoshiasha A., Okuba M., Nakatani T., Hayasaka Y., and Isobe H. (2013)
683 Local structure of Titanium in natural glasses probed by X-ray absorption fine
684 structure. Journal of Physics Conference Series, 430, 012121.
685 Waychunas G.A. (1987) Synchrotron radiation XANES spectroscopy of Ti in minerals:
686 effects of Ti bonding distance, Ti valence, and site geometry on absorption edge
687 structure. American Mineralogist, 72, 89-101.
688 Weeks R.A., Underwood J.R., Glegengack R. (1984) Libyan Desert glass: a review.
689 Journal of Non-Crystalline Solids, 67, 593-619,
690 Wilding M., Webb S., and Dingwell D.B. (1996a) Tektite cooling rates: Calorimetric

691 relaxation geospeedometry applied to a natural glass. Geochimica et Cosmochimica
692 Acta, 60, 1099-1103.
693 Wilding M., Webb S., Dingwell D.B., Abley G., and Marti J. (1996b) Cooling rate
694 variation in natural volcanic glasses from Tenerife, Canary Islands. Contributions to
695 Mineralogy and Petrology, 125, 151-166.
696 Wright A.C., Desa J.A.E., Week R.A., Sinclair R.N., and Bailey D.K. (1984) Neutron
697 diffraction studies of natural glasses. Journal of Non-Crystalline Solids, 6**7,** 35-44.
698 Yarker C.A., Johnson P.A.V., Wright A.C., Wong J., Greegor R.B., Lytle F.W., and
699 Sinclair, R.N. (1986) Neutron diffraction and EXAFS evidence for TiO_5 units in
700 vitreous $K_2O{\cdot}TiO_2{\cdot}2SiO_2$. Journal of Non-Crystalline Solids, 79, 117-136.
701 Yoshiasa A., Nagai T., Ohtaka O., Kamishima O. and Shimomura O. (1999) Pressure
702 and temperature dependence of EXAFS Debye-Waller factors in diamond-type and
703 white-tin-type germanium. Journal of Synchrotron Radiation, 6, 43-49.
704 Žak K., Skála R., Řanda Z., Mizera J., Heissig K., Ackerman L., Ďurisova J., Jonášová
705 Š., Kameník J., and Magna T. (2016) Chemistry of tertisry sediments in the
706 surrounding of the Ries impact structure and moldavite formation revisited.
707 Geochimica et Cosmochimica Acta, 179, 287-311.
708

709 **Figure captions**

710 Fig. 1. An illustration of our shock recovery experimental setup.
711 Fig. 2. Impedance match diagram to estimate pressures at four impact velocities of case
712 A for 0.899 km/s of Al6061 (3 mm thick), case B for 0.981 km/s and case C for
713 1.386 km/s of SUS304 (2 mm thick), and case D for 1.400 km/s of W (2 mm thick).

(a) The first pressures are at points A1, B1, C1, and D1 and then the pressures increase stepwise with time as indicated by arrows at A1, C1, and D1, respectively. Case B is not illustrated. (b) Numbers of reflection is 3 to 4 at the middle central section of sample. Pressure reaches a peak at ~1.4 μs and drops subsequently, as calculated by Autodyne code.

Fig. 3. Comparison of X-ray diffraction patterns at 2θ of 15-35 degrees for the starting tektite (TK0) and recovered samples (TK1, TK2, TK3, TK4, TKP1, and TKP2) by Cu Kα radiation.

Fig. 4. Comparison of Raman spectra for the starting tektite (TK0) and recovered samples (TK1, TK2, TK3, TK4, TKP1, and TKP2). Line colors are same as in Fig. 3.

Fig. 5. Ti K-edge XANES spectra for the starting tektite (TK0) and recovered samples (TK1, TK2, TK3, TK4, TKP1, and TKP2) (a) and their expansions around 4.97 KeV (b). Reference materials are compared in (a). Intensity is normalized to the highest one for comparison. Line colors are same as in Fig. 3.

Fig. 6. Relationship between the Ti-O distance and pre-edge position for Ti K XANES for the shocked tektites (TK0, TK1, TK2, TK3, TK4, TKP1, and TKP2), selected natural glasses (ti-t7 for tektites, m1-m2 for impact glasses, and v1-v2 for volcanic glasses), and references (TiO_2 (rutile), Ti_2O_3 (corundum), and γ-TiO). Energy is calibrated by the Ti metal (4964.9 eV). Three widths for [IV], [V], and [VI] show energy rages of the corresponding coordination numbers (CN) of Ti^{4+} in measured silicate glasses (Ackerson et al., 2020), respectively. Arrows (1) and (2) illustrate trends of increasing CN for Ti^{4+} and Ti^{3+} in silicate glasses, respectively. Data for

737 tektites (t1 indochinite, t2 moldavite-brownish, t3 bediasite, t4 hainanite-rim, t5
738 australite, t6 philippinite, and t7 moldavite-green), impact glasses (m1 suevite and
739 m2 impactite), and volcanic glasses (v1 obsidian and v2 Kilauea volcanic glass) from
740 Wang et al. (2011 and 2013) are listed in Table S1. TiO_2 (rutile) from Table 3. The
741 average Ti-O distances for Ti_2O_3 and TiO phases from Hwang et al. (2016) and
742 Amano et al. (2016), respectively. Note two distinct trends to TiO_2 for Ti^{4+} and Ti_2O_3
743 for Ti^{3+} from the area of the tetrahedral Ti^{4+} (1.81-1.85 Å and ~4968 eV) with
744 increasing the average Ti-O distance.

745 Table 1.

746 Chemical compositions (wt %) of tektite used in the present study,

747 compared with those of australite.

748

	Tektite (TK0)	Thailande	Average Australasian
SiO_2	73.92	72.3	70.70 ± 4.53
TiO_2	0.76	0.9	0.68 ± 0.15
Al_2O_3	12.67	12.9	13.23 ± 2.42
CaO	2.06	1.9	3.77 ± 0.96
MgO	1.87	1.9	2.48 ± 1.31
FeO	4.39	4.4	4.64 ± 0.86
Fe_2O_3			0.64 ± 0.29
MnO	0.09	0.1	0.10 ± 0.01
K_2O	2.44	2.5	2.03 ± 0.54
Na_2O	1.21	1.2	1.63 ± 0.89
ZrO_2	0.03	-	-
Total	99.44	98.1	
Ref.	This study	Farges and Brown (1997)	Glass (2016)

749

750

751 Table 2.

752 Experimental conditions of shock recovery experiments on tektite (TK0) and calculated peak
753 pressures, density, and post-shock temperatures.

754

Sample (thickness, mm)	Flyer (thickness, mm)	Impact velocity (km/s)	Peak states for Pressure (GPa)	Density (g/cm^3)	Post-shock Temperature (K)
TK1 (1.13)	Al6061 (3)	0.899	10	2.68	440
TK2 (1.14)	SUS304 (2)	0.981	17	3.23	1170
TK3 (1.17)	SUS304 (2)	1.386	23	4.10	2100
TK4 (1.17)	W (2)	1.400	35	5.91	2140
TKP1 (1.39)	SUS304 (2)	0.671	13	-	1070
TKP2 (1.63)	SUS304 (2)	1.510	34	-	2390

755

756

Table 3.

Summary of XAFS measurements of Ti K pre-edge peak for shocked sample and reference materials.

Sample	Pre-edge peak		Ti-O distance	R-factor
	Position (eV)	Intensity (%)	(Å)	(%)
TK0	4967.9	50	1.844 (3)	0.1
TK1	4968.0	52	1.841 (1)	9.7
TK2	4968.5	42	1.844 (5)	2.1
TK3	4968.5	34	1.913 (5)	0.3
TK4	4969.7	12	1.965 (4)	0.4
TKP1	4967.9	43	1.872 (3)	9.9
TKP2	4967.9	49	1.8880 (8)	1.0
Ti-foil	4964.9	-	-	-
TiO_2-rutile	4970.0	10	1.975 (3)	1.3
Ti_2O_3-corundum	4967.4-4968.2		2.048 (15)	
γ-TiO	4966.9-4967.7		2.092	

The listed Ti K pre-edge positions were determined and the estimation of Ti-O distance is reliable if R-factor is lower than 10 % in the present XAFS study. The Ti-O distances for γ-TiO (NaCl-type) and corundum-type Ti_2O_3 are cited from Amano et al. (2016) and Hwang et al. (2016), respectively.

This is the peer-reviewed, final accepted version for American Mineralogist, published by the Mineralogical Society of America.
The published version is subject to change. Cite as Authors (Year) Title. American Mineralogist, in press.
DOI: https://doi.org/10.2138/am-2022-8149. http://www.minsocam.org/

Fig. 1

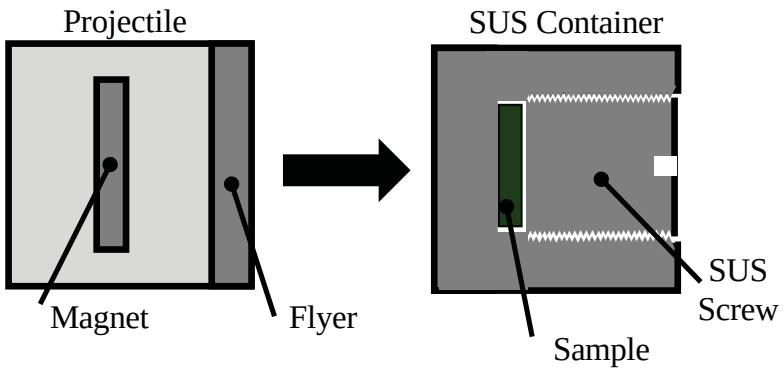

This is the peer-reviewed, final accepted version for American Mineralogist, published by the Mineralogical Society of America.
The published version is subject to change. Cite as Authors (Year) Title. American Mineralogist, in press.
DOI: https://doi.org/10.2138/am-2022-8149. http://www.minsocam.org/

Fig. 2

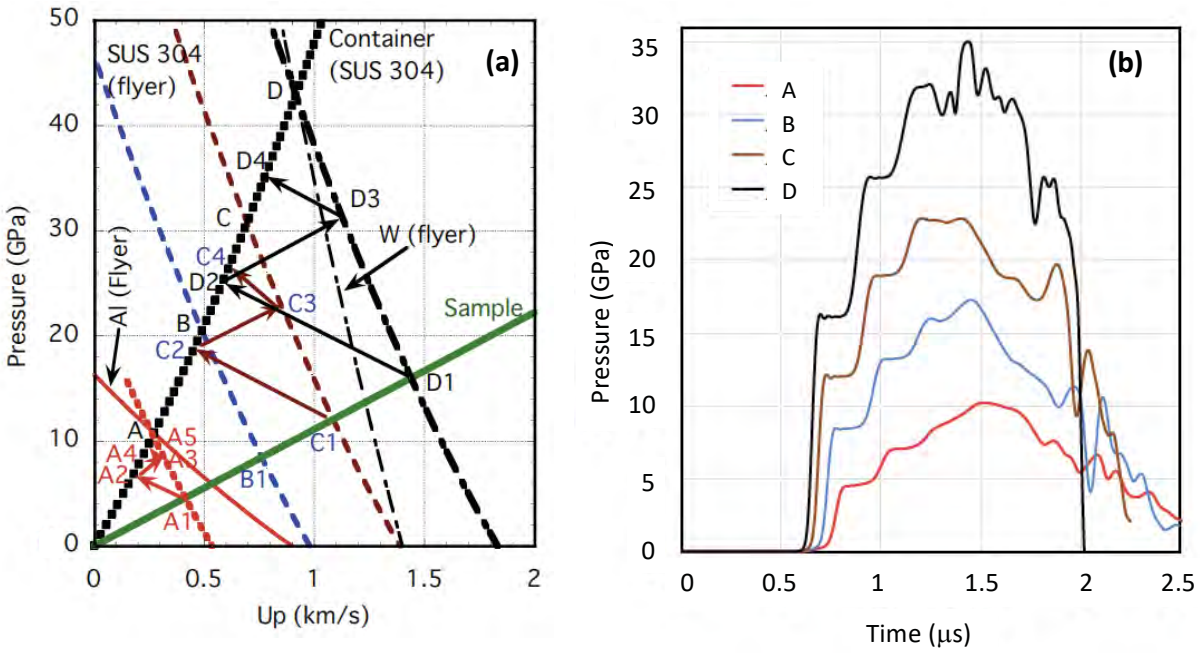

This is the peer-reviewed, final accepted version for American Mineralogist, published by the Mineralogical Society of America.
The published version is subject to change. Cite as Authors (Year) Title. American Mineralogist, in press.
DOI: https://doi.org/10.2138/am-2022-8149. http://www.minsocam.org/

Fig. 3

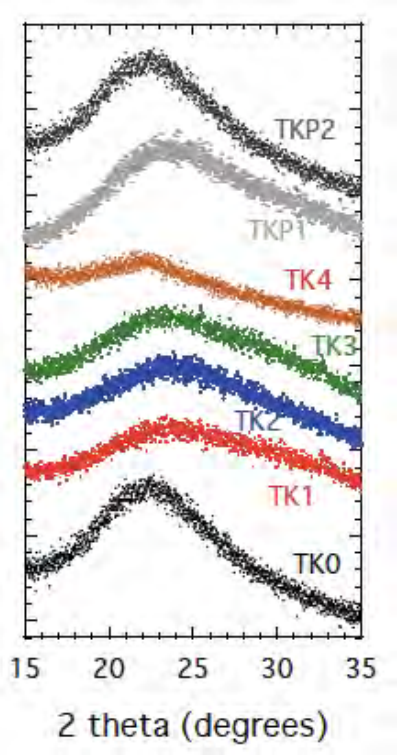

This is the peer-reviewed, final accepted version for American Mineralogist, published by the Mineralogical Society of America.
The published version is subject to change. Cite as Authors (Year) Title. American Mineralogist, in press.
DOI: https://doi.org/10.2138/am-2022-8149. http://www.minsocam.org/

Fig.4

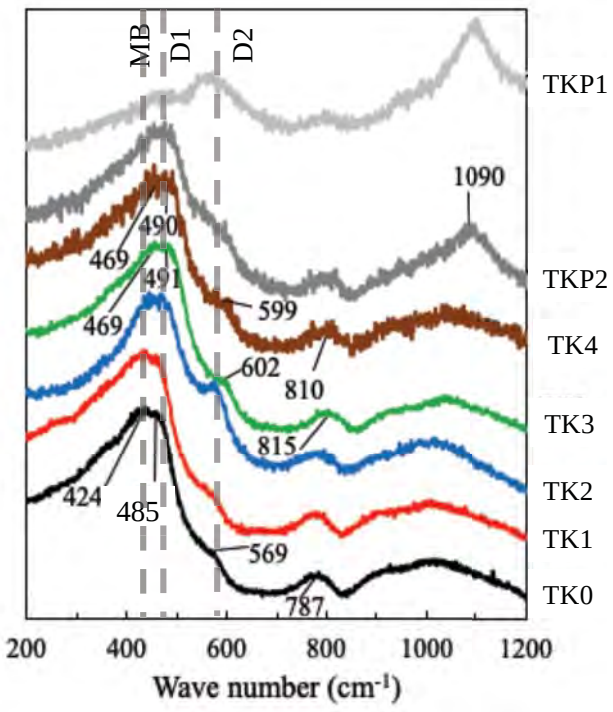

This is the peer-reviewed, final accepted version for American Mineralogist, published by the Mineralogical Society of America.
The published version is subject to change. Cite as Authors (Year) Title. American Mineralogist, in press.
DOI: https://doi.org/10.2138/am-2022-8149. http://www.minsocam.org/

Fig. 5

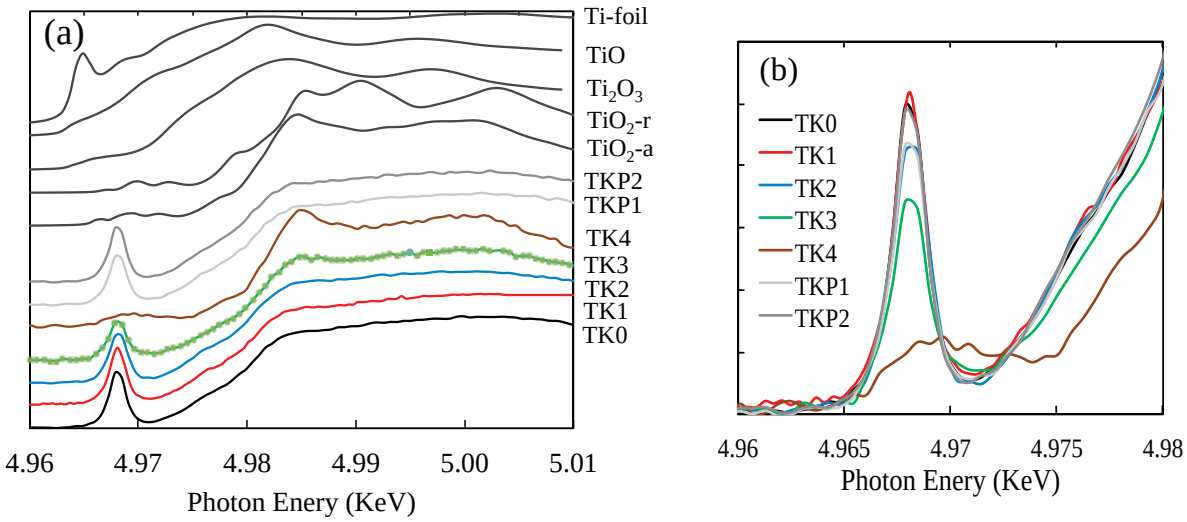

This is the peer-reviewed, final accepted version for American Mineralogist, published by the Mineralogical Society of America.
The published version is subject to change. Cite as Authors (Year) Title. American Mineralogist, in press.
DOI: https://doi.org/10.2138/am-2022-8149. http://www.minsocam.org/

Fig. 6